

Article

# High-quality-factor optical microresonators fabricated on lithium niobite thin film with an electro-optical tuning range spanning over one free spectral range

Zhe Wang<sup>1,2,3,†</sup>, Chaohua Wu<sup>4,5,†</sup>, Zhiwei Fang<sup>6,7,\*</sup>, Min Wang<sup>6,7</sup>, Jintian Lin<sup>1</sup>, Rongbo Wu<sup>1,2</sup>, Jianhao Zhang<sup>1,2</sup>, Jianping Yu<sup>1,2</sup>, Miao Wu<sup>6,7</sup>, Wei Chu<sup>7</sup>, Tao Lu<sup>8</sup>, Gang Chen<sup>4,5,\*</sup> and Ya Cheng<sup>1,5,6,7,\*</sup>

<sup>1</sup> State Key Laboratory of High Field Laser Physics and CAS Center for Excellence in Ultra-intense Laser Science, Shanghai Institute of Optics and Fine Mechanics(SIOM), Chinese Academy of Sciences(CAS), Shanghai 201800, China; 1164087017@qq.com(Z.W.) ; jintianlin@siom.ac.cn (J.L.); rbwu@siom.ac.cn (R.W.); jhzhang@siom.ac.cn (J.Z.); 1910758@tongji.edu.cn(J.Y.)

<sup>2</sup> Center of Materials Science and Optoelectronics Engineering, University of Chinese Academy of Sciences, Beijing 100049, China

<sup>3</sup> School of Physical Science and Technology, ShanghaiTech University, Shanghai 200031, China

<sup>4</sup> State Key Laboratory of Quantum Optics and Quantum Optics Devices, Institute of Laser Spectroscopy, Shanxi University, Taiyuan 030006, China; sxwuchua@163.com(C.W.)

<sup>5</sup> Collaborative Innovation Center of Extreme Optics, Shanxi University, Taiyuan 030006, China

<sup>6</sup> State Key Laboratory of Precision Spectroscopy, East China Normal University, Shanghai 200062, China; mawang@phy.ecnu.edu.cn (M.W.); wumiao1993@126.com(M.W.)

<sup>7</sup> The Extreme Optoelectromechanics Laboratory (XXL), School of Physics and Materials Science, East China Normal University, Shanghai 200241, China; wchu@phy.ecnu.edu.cn(W.C.)

<sup>8</sup> Department of Electrical and Computer Engineering, University of Victoria, Victoria, BC, V8P 5C2, Canada; taolu@ece.uvic.ca (T.L.)

\* Corresponding author: zwfang@phy.ecnu.edu.cn(Z.F.); gangchen@zjut.edu.cn(G.C.); ya.cheng@siom.ac.cn(Y.C.)

† These authors contributed equally to this paper.

**Abstract:** We demonstrate high quality (intrinsic Q factor  $\sim 2.8 \times 10^6$ ) racetrack microresonators fabricated on lithium niobate (LN) thin film with a free spectral range (FSR) of  $\sim 86.38$  pm. By integrating microelectrodes alongside the two straight arms of the racetrack resonator, the resonance wavelength around the 1550 nm can be red shifted by 92 pm when the electric voltage is raised from -100 V to 100 V. The microresonators of the tuning range spanning over a full FSR is fabricated using photolithography assisted chemo-mechanical etching (PLACE).

**Keywords:** microresonators; lithium niobate; electro-optical tuning; chemo-mechanical etching

## 1. Introduction

Whispering gallery mode (WGM) optical microresonators play a crucial role in both photonic research and applications owing to the strong confinement of light fields resulting from the characteristic high quality (Q) factors [1]. Currently, most optical microresonators

fabricated on chip have a footprint below 1 mm. Such small microresonators can be fabricated on various types of materials such as silica [2], semiconductors [3], crystals [4], and polymers [5] using lithographic techniques. The integrated microresonators have enabled a broad range of functionalities including filtering, wavelength conversion, sensing, optomechanics, and comb generation [6,7]. However, for some applications such as Brillouin lasers [8,9], optical-frequency synthesizer [10], microwave photonics [11], spectroscopy [12], gyroscope sensors [13], optical atomic clock [14], and high-resolution spectrometers [15], WGM microresonators with perimeters up to centimeter level are desirable. Fabrication of such large microresonators using lithographic techniques is challenging. Usually, ultra-violet (UV) lithography cannot directly define such large microresonators, thus stitching is frequently employed to meet the size requirement [16]. Nevertheless, stitching can inevitably cause fabrication errors, which will spoil the Q. On the other hand, electron beam lithography (EBL) and focused ion beam (FIB) milling are both low-throughput fabrication techniques as compared to optical lithography technology [17,18]. It is time consuming to fabricate the large WGM microresonators using the EBL and FIB although high fabrication resolutions are readily achievable with the two techniques. For these reasons, advanced lithographic techniques should be developed to meet the requirements on both fabrication resolution and efficiency.

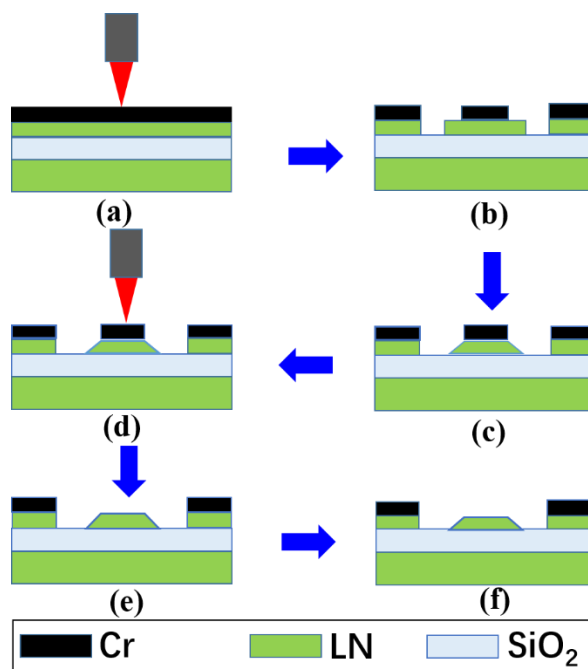
Here, we demonstrate high quality optical microresonators fabricated on lithium niobate (LN) thin film with an electro-optical (EO) tuning range spanning over one free spectral range. The advantage of choosing LN as the substrate material is the strong electro-optic property. In particular, our fabrication technique based on photolithography assisted chemo-mechanical etching (PLACE) allows to define the mask pattern of a racetrack WGM resonator with a footprint size of 1.2 cm×5.2 cm in only ~1 hr. The fabricated device shows an intrinsic Q factor of  $2.8 \times 10^6$ . We also integrate microelectrodes alongside the two straight arms of the racetrack resonator. We examine the EO tunability and tuning range of the microresonator. We observe that when the electric voltage is raised from -100 V to 100 V, the resonance wavelength around the 1550 nm can be red tuned by 92 pm, which exceeds the free spectral range (FSR~86.38 pm) of the fabricated microresonator.

## 2. Materials and Methods

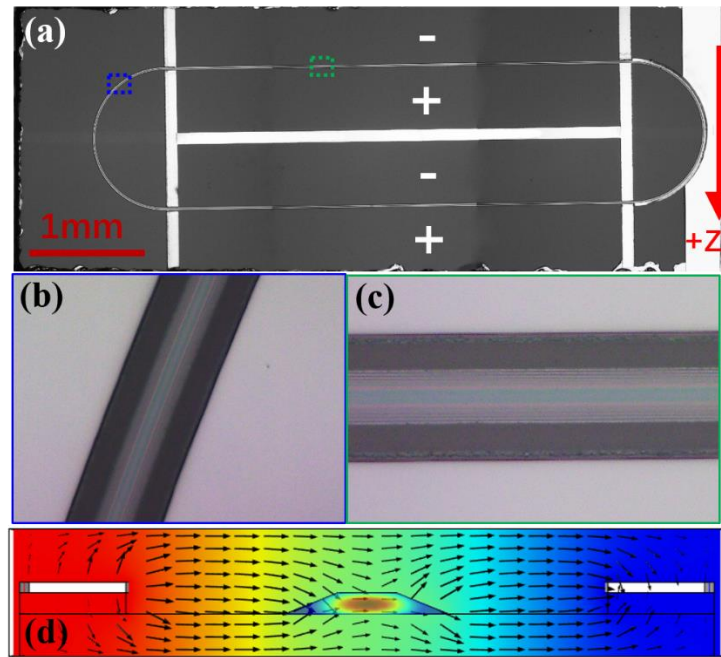
In our experiment, the on-chip LN racetrack resonator integrated with Cr electrodes was fabricated on a commercially available X-cut LN on insulator (LNOI) wafer (NANOLN, Jinan Jingzheng Electronics Co. Ltd.). The LN thin film with a thickness of 900 nm was bonded onto a silica layer with a thickness of ~2  $\mu\text{m}$ , and the silica layer was grown on a 0.5 mm-thick LN substrate. A 600-nm-thick chromium (Cr) film was further deposited on the top surface of LNOI by magnetron sputtering. The fabrication process includes four steps, as illustrated in Fig. 1. Firstly, the Cr film on the LNOI sample was patterned into a stripe-shaped mask using space-selective femtosecond laser (PHAROS, LIGHT CONVERSION Inc.). Subsequently, the chemo-mechanical polishing (CMP) process was performed to fabricate the LN waveguide using a wafer polishing machine (NUIPOL802, Kejing Inc.). The LN thin film protected by the Cr mask was preserved after the CMP process whereas the remaining LN in the opening area was completely removed. This step allows to create LN waveguides with extremely smooth sidewalls, ensuring high Q factors for the fabricated microresonators [19-21]. Next, the femtosecond laser ablation was carried out again to remove the Cr mask left behind on the LN

waveguides. Finally, a post-CMP process was performed for thinning the LN disk and smoothing the top surface. In the current experiment, the fabricated ridge waveguides have a top width of  $\sim 2 \mu\text{m}$ , and the Cr electrodes on the two sides of the waveguide are separated by a distance of  $\sim 20 \mu\text{m}$ . It takes about 1 hr in total to produce the whole racetrack microresonator as shown in Fig. 2(a). The microelectrodes were fabricated by patterning the Cr film using the femtosecond laser micromachining.

Figure 2(a) presents the top view of the on-chip LN racetrack resonator integrated with the Cr electrodes. The diameter of the two half circles of the racetrack resonator is 1.2 mm, and the length of straight arms of the racetrack is 4 mm. Therefore, the perimeter of the microresonator is  $\sim 11.77 \text{ mm}$ . Figure 2(b) and (c) presents the zoom-in images of the curved and straight waveguides of the LN racetrack resonator, respectively. Figure 2(d) shows the numerically simulated optical and electric fields overlapping each other. Since the device was fabricated on an X-cut LN wafer, the transverse-electric (TE) optical modes can be efficiently tuned thanks to the highest electro-optic tensor component ( $r_{33}$ ) of LN.



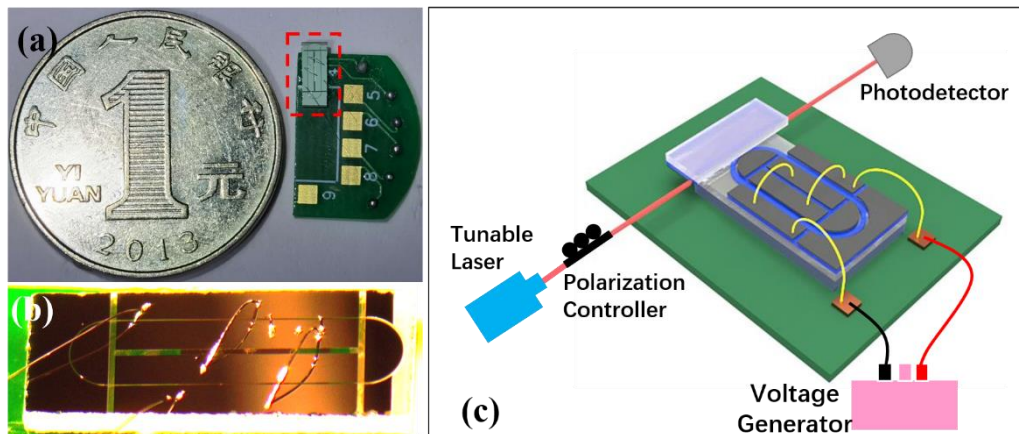
**Figure 1.** Process flow of fabricating an on-chip LN racetrack resonator integrated with Cr microelectrodes. (a)-(b) Patterning the Cr thin film into a stripe mask using femtosecond laser microfabrication. (c) Etching of the LNOI layer by chemo-mechanical polishing. (d)-(e) Selective removal of the stripe Cr mask on the LN racetrack resonator using femtosecond laser ablation. (f) Reducing the thickness of LN racetrack resonator by a post chemo-mechanical polishing, which leads to the smooth top surface on the LN waveguide.



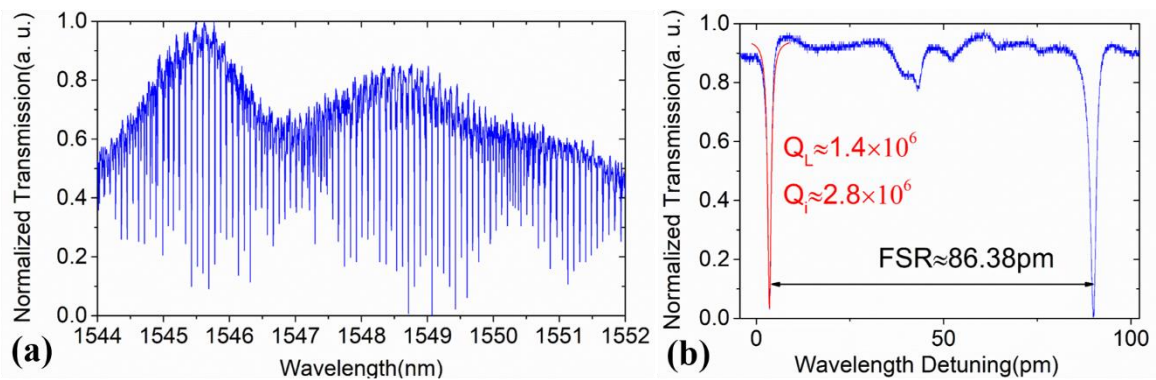
**Figure 2.** (a) Top view optical micrograph of the on-chip LN racetrack resonator integrated with Cr electrodes. Zoom-in optical micrograph of the curved (b) and (c) straight waveguides. (d) Distributions of optical (TE) field and electrical field overlapping each other simulated using COMSOL. The arrows indicate the direction of the electric field.

### 3. Results

Figure 3(a) presents the digital-camera-captured picture of the racetrack resonator as compared with a one-yuan Renminbi coin. The zoom-in optical micrograph in Fig. 3(b) further shows the details of the racetrack resonator and the Cr electrodes as well as the aluminium wire (diameter~25 $\mu$ m) connecting the Cr electrodes to the voltage generator. To characterize the tunability of the LN racetrack resonator, we used an experimental setup as illustrated in Fig. 3(c). Here, a tunable laser (LTB-6728, Newport Inc.) was used as the light source. To enable efficient coupling of the light into the racetrack microresonator, we first fabricated a straight waveguide on another LNOI wafer. The straight waveguide has the same geometric parameters such as the cross sectional shape, thickness and width as that of the waveguide in the LN racetrack resonator. The light from the tunable laser was coupled into the straight waveguide using a lensed fiber. The straight waveguide was then brought close to the racetrack resonator from the top to allow for evanescent coupling as shown in Fig. 3(c). Due to the same geometric parameters of the straight waveguide and the racetrack waveguide, phase matching can be ensured to enable efficient coupling between them. The polarization state of the input light was adjusted using an in-line fiber polarization controller. The output of the LN waveguide was connected to a photodetector (New focus 1811-FC-AC, Newport Inc.) using a lensed fiber for measuring the transmission spectrum and the Q factor of the racetrack resonator. A programmable linear direct current (DC) stabilized power source (IPMP500-0.6L, INTERLOCK Technologies Inc.) was used as the voltage generator, which provided a variable voltage ranging from -100 V to 100 V.

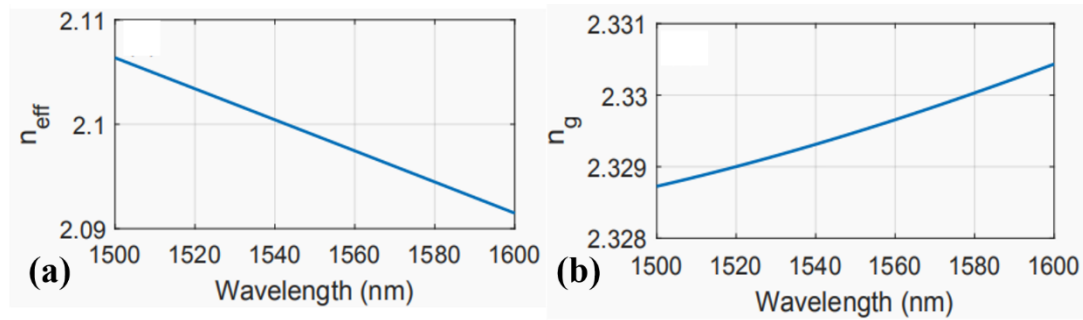


**Figure 3.** (a) Picture of the LN racetrack resonator integrated with Cr electrodes. (b) Zoom-in image of the LN racetrack resonator integrated with Cr electrodes. (c) Schematic of the experimental setup for characterizing the Q factor and tunability of the device.



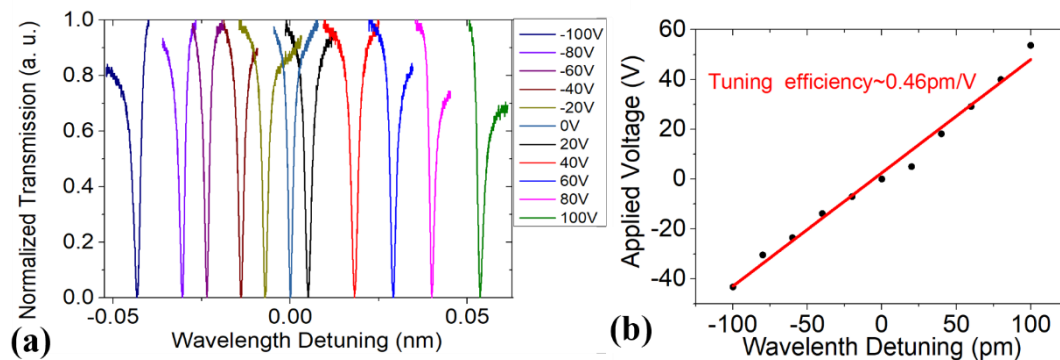
**Figure 4.** (a) Transmission spectrum of the LN racetrack resonator. (b) The Lorentz fitting (red curve) reveals a loaded Q factor of  $1.4 \times 10^6$ , corresponding to an intrinsic Q factor of  $2.8 \times 10^6$  as measured at 1547.93 nm wavelength.

Figure 4(a) shows the measured transmission spectrum in the wavelength range between 1544 and 1552 nm. The resonance lines appeared regularly spaced, indicating that mostly the fundamental mode is excited in the LN racetrack resonator. This should be a result of the same geometric parameters of the upper straight waveguide and the lower racetrack waveguide as shown in Fig. 3(c). In this case, the spatial mode profiles in the two waveguides can most efficiently overlap. Thus, as the fundamental mode is excited in the upper waveguide with the lensed fiber, the same fundamental mode will be excited in the racetrack resonator as well. As shown in Fig. 4(b), the FSR of the microresonator was determined to be 86.38 nm. One of the WGM at the resonant wavelength of 1547.93 nm was chosen for the measurement of the loaded quality factor QL. By fitting with the Lorentz function, QL is determined to be  $1.4 \times 10^6$ , which corresponds to an intrinsic quality factor  $Q_i \sim 2.8 \times 10^6$  as evidenced by the critical coupling characteristic (i.e., the very deep dips in the transmission spectrum) in Fig. 4(b).



**Figure 5.** (a) The calculated effective index  $n_{eff}$  and (b) group index  $n_g$  of the optical mode in Fig. 2(d) for the wavelength range between 1550 and 1600 nm.

Numerical simulations were performed using COMSOL to reveal the optical mode profile in our LN waveguide (see, Fig. 2(d)). In particular, the calculated effective index  $n_{eff}$  and group index  $n_g$  as functions of the wavelength are shown in Figs. 5(a) and (b), respectively. At the wavelength of 1550 nm,  $n_{eff}$  and  $n_g$  are calculated to be  $\sim 2.098$  and  $\sim 2.329$ , respectively. In combination with the experimentally determined perimeter of our LN racetrack of  $\sim 11.77$  mm, it can be derived that  $FSR \approx 87.6$  pm. The theoretical simulated FSR agrees well with our experimentally measured FSR (86.38 pm).



**Figure 6.** (a) The resonance wavelength continuously red shifts with the increasing voltage. (b) The linearly fitting reveals an electrical tuning efficiency of  $\sim 0.46$  pm/V and indicates that the tuning range spans over a full FSR.

Finally, we carried out the real-time tuning of the racetrack microresonator by adding a tunable electric voltage on the Cr microelectrodes. Figure 6(a) shows a group of transmission spectra recorded near the 1550 nm wavelength at various electric voltages in the range of -100 V and +100 V with a voltage tuning step of 20 V. We observe that by increasing the electric voltage from -100 V to +100 V, the resonance wavelength can be continuously red tuned by  $\sim 92$  pm, which spans over one FSR ( $\sim 86.38$  pm). The fitting line in Fig. 6(b) indicates a linear dependence of the resonance wavelength on the applied electric voltage and a tuning rate of  $\sim 0.46$  pm/V.

#### 4. Discussions

This is the first attempt of fabricating a large WGM microresonator on LNIOI using the PLACE fabrication technique. Before, we have shown that freestanding microdisks of diameters of  $\sim 100$   $\mu\text{m}$  fabricated on the LNOI substrates using the PLACE technique can easily

achieve Q factors above  $10^7$  [19,21]. Here, the racetrack microresonator shows a Q factor nearly one order of magnitude lower. Most likely, this is caused by the scratches and defects which can be more easily generated on large photonic structures during the chemo-mechanical polishing. This suggests that more stringent control on the polishing and sample cleaning processes is necessary for maintaining the high Qs in the fabrication of the large microresonators. In principle, the sub-nanometer surface roughness provided by the PLACE fabrication technique is sufficient to support Q factors above  $10^7$  for the large microresonators. We also notice that the EO tuning efficiency of 0.46 pm/V is lower in comparison with the results reported in the recent literatures [22,23]. This is because the waveguide designed in this work has been optimized for dispersion engineering, which features a relatively broad width at the bottom of the waveguide ( $\sim 7 \mu\text{m}$ ). Thus, the two electrodes on the two sides of the waveguides are separated from each other by  $\sim 20 \mu\text{m}$ , which is the main cause of the relatively low tuning efficiency. However, in the current work, our goal is to achieve the large tuning range covering the full FSR but not the high-speed EO modulation. The demonstrated tuning efficiency is sufficiently high for such application.

## 5. Conclusions

To conclude, we have demonstrated high Q optical microresonators fabricated on LN thin film with an EO tuning range spanning over a full FSR. The EO tunable racetrack resonator of the perimeter above 1 cm features an FSR of  $\sim 86.38 \text{ nm}$ , an intrinsic Q factor of  $\sim 2.8 \times 10^6$ , and an EO tuning efficiency of 0.46 pm/V. The device provides a technological platform for a range of applications such as filtering, microwave photonics, sensing, and information processing.

**Author Contributions:** conceptualization, Y.C.; methodology, Z.F., and Y.C.; investigation, Z.W., C.W. and Z.F.; software, Z.W. and Z.F.; formal analysis, Z.W., C.W., M. W.(Miao Wu), J. Y., and Z.F.; Data Curation, Z.F., W.C., and J.L.; validation, Z.F., W.C., and J.L.; resources, Z.W., C.W., Z.F., R.W., and J.Z.; writing-original draft preparation, Z.W., C.W., M. W.(Min Wang), and Z.F.; writing-review and editing, T.L., G.C., and Y.C.; visualization, Z.F., W.C., and J.L.; supervision, G.C. and Y.C.; funding acquisition, T.L., and Y.C.; project administration, M. W.(Min Wang), and Y.C.; All authors have read and agreed to the published version of the manuscript.

**Funding:** This research was funded by the National Key R&D Program of China (2019YFA0705000, 2018YFB2200400), National Natural Science Foundation of China (Grant Nos. 11822410, 11874154, 11874375, 11734009, 61761136006, 11674340, 61675220, 61590934), the Strategic Priority Research Program of Chinese Academy of Sciences (Grant No. XDB16030300), the Key Project of the Shanghai Science and Technology Committee (Grant Nos. 18DZ1112700, 17JC1400400), Shanghai Municipal Science and Technology Major Project (Grant No.2019SHZDZX01), the Shanghai Pujiang Program (Grant No. 18PJ1403300), the Shanghai Rising-Star Program (Grant No. 17QA1404600), the Key Research Program of Frontier Sciences, Chinese Academy of Sciences (Grant No. QYZDJ-SSW-SLH010), and the Fundamental Research Funds for the Central Universities (2018FZA5004), Nature Science and Engineering Research Council of Canada (NSERC) Discovery (Grant No. RGPIN-2020-05938).

**Acknowledgments:** We thank Dr. Rui Zhu and Prof. Qingfeng Zhan from East China Normal University for their technical support.

**Conflicts of Interest:** The authors declare no conflict of interest.

## References:

1. Vahala, K. J.; Optical microcavities. *Nature* **2003**, *424*, 839–846.
2. Cai, M.; Painter, O.; Vahala, K. J.; Observation of critical coupling in a fiber taper to a silica-microsphere whispering-gallery mode system. *Phys. Rev. Lett.* **2000**, *85*, 74–77.

3. Soltani, M.; Yegnanarayanan, S.; Adibi, A.; Ultra-high Q planar silicon microdisk resonators for chip-scale silicon photonics. *Opt. Express* **2007**, *15*, 4694-4704.
4. Lin, J.; Xu, Y.; Fang, Z.; Wang, M.; Song, J.; Wang, N.; Qiao, L.; Fang, W.; Cheng, Y. Fabrication of high-Q lithium niobate microresonators using femtosecond laser micromachining. *Sci. Rep.* **2015**, *5*, 8072.
5. Kuwata-Gonokami, M. ; Jordan, R. H.; Dodabalapur, A.; Katz, H. E.; Schilling, M. L.; Slusher, R. E.; Ozawa, S.; Polymer microdisk and microring lasers. *Opt. Lett.* **1995**, *20*, 2093-2095.
6. Ward, J.; Benson, O.; WGM microresonators: sensing, lasing and fundamental optics with microspheres. *Laser Photonics Rev.* **2011**, *5*, 553-570.
7. Gaeta, A. L.; Lipson, M.; Kippenberg, T. J.; Photonic-chip-based frequency combs. *Nat. Photonics* **2019**, *13*,158.
8. Lee, H.; Chen, T.; Li, J.; Yang, K. Y.; Jeon, S.; Painter, O.; Vahala, K. J.; Chemically etched ultrahigh-Q wedge-resonator on a silicon chip. *Nat. Photonics* **2012**, *6*, 369.
9. Yang, K. Y.; Oh, D. Y.; Lee, S. H.; Yang, Q. F.; Yi, X. ; Shen, B.; Wang, H.; Vahala, K.; Bridging ultrahigh-Q devices and photonic circuits. *Nat. Photonics* **2018**, *12*, 297-302.
10. Liu, J.; Lucas, E.; Raja, A. S.; He, J.; Riemensberger, J.; Wang, R. N.; Karpov, M.; Guo, H.; Bouch, R.; Kippenberg, T. J.; Photonic microwave generation in the X-and K-band using integrated soliton microcombs. *Nat. Photonics* **2020**, 1-6.
11. Spencer, D. T.; Drake, T.; Briles, T. C.; Stone, J.; Sinclair, L. C.; Fredrick, C.; Li, Q.; Westly, D.; Robert Ilic, B.; Bluestone, A.; Volet, N.; Komljenovic, T.; Chang, L.; Lee, S. H.; Oh, D. Y.; Suh, M.G.; Yang, K. Y.; Pfeiffer, M. H. P.; Kippenberg, T. J.; Norberg, E.; Theogarajan, L.; Vahala, K.; Newbury, N. R.; Srinivasan, K.; Bowers, J. E.; Diddams, S. A.; Papp, S. B.; An optical-frequency synthesizer using integrated photonics. *Nature* **2018**, *557*, 81-85.
12. Suh, M. G.; Yang, Q. F.; Yang, K. Y.; Yi, X.; Vahala, K. J.; Microresonator soliton dual-comb spectroscopy. *Science* **2016**, *354*, 600-603.
13. Li, J.; Suh, M. G.; Vahala, K.; Microresonator brillouin gyroscope. *Optica* **2017**, *4*, 346-348.
14. Newman, Z. L.; Maurice, V.; Drake, T.; Stone, J. R.; Briles, T. C.; Spencer, D. T.; Fredrick, C.; Li, Q.; Westly, D.; Ilic, B. R.; Shen, B.; Suh, M.; Yang, K. Y.; Johnson, C.; Johnson, D. M. S.; Hollberg, L.; Vahala, K. J.; Srinivasan, K.; Diddams, S. A.; Kitching, J.; Papp, S. B.; Hummon, M. T.; Architecture for the photonic integration of an optical atomic clock. *Optica* **2019**, *6*, 680-685.
15. Yang, Q. F.; Shen, B.; Wang, H.; Tran, M.; Zhang, Z. Yang, K. Y.; Wu, L.; Bao, C.; Bowers, J.; Yariv, A.; Vahala, K.; Vernier spectrometer using counterpropagating soliton microcombs. *Science* **2019** *363*, 965-968.
16. Wang, J.; Bo, F.; Wan, S.; Li, W.; Gao, F.; Li, J.; Zhang, G.; Xu, J.; High-Q lithium niobate microdisk resonators on a chip for efficient electro-optic modulation. *Opt. express* **2015**, *23*, 23072-23078.
17. Zhang, M.; Buscaino, B.; Wang, C.; Shams-Ansari, A.; Reimer, C.; Zhu, R.; Kahn, J. M.; Lončar, M.; Broadband electro-optic frequency comb generation in a lithium niobate microring resonator. *Nature* **2019**, *568*, 373-377.
18. Fang, Z.; Xu, Y.; Wang, M.; Qiao, L.; Lin, J.; Fang, W.; Cheng, Y.; Monolithic integration of a lithium niobate microresonator with a free-standing waveguide using femtosecond laser assisted ion beam writing. *Sci. Rep.* **2017**, *7*, 45610.
19. Wu, R.; Zhang, J.; Yao, N.; Fang, W.; Qiao, L.; Chai, Z.; Lin, J.; Cheng, Y.; Lithium niobate micro-disk resonators of quality factors above  $10^7$ . *Opt. Lett.* **2018**, *43*, 4116-4119.
20. Wu, R.; Wang, M.; Xu, J.; Qi, J.; Chu, W.; Fang, Z.; Zhang, J.; Zhou, J.; Qiao, L.; Chai, Z.; Lin, J.; Cheng, Y.; Long Low-Loss-Lithium Niobate on Insulator Waveguides with Sub-Nanometer Surface Roughness. *Nanomaterials* **2018**, *8*, 910.
21. Fang, Z.; Luo, H.; Lin, J.; Wang, M.; Zhang, J.; Wu, R.; Zhou, J.; Chu, W.; Lu, T.; Cheng, Y.; Efficient electro-optical tuning of an optical frequency microcomb on a monolithically integrated high-Q lithium niobate microdisk, *Opt. Lett.* **2019**, *44*, 5953-5956.
22. Wang, C.; Zhang, M.; Stern, B.; Lipson, M.; Lončar, M.; Nanophotonic lithium niobate electro-optic modulators. *Opt. Express* **2018**, *26*, 1547-1555.
23. Wang, T. J.; Peng, G. L.; Chan, M. Y.; Chen, C. H.; On-Chip Optical Microresonators With High Electro-Optic Tuning Efficiency. *J. Lightwave Technol.* **2020**, *38*, 1851-1857.